Ocean Engineering 261 (2022) 112186

Contents lists available at ScienceDirect

Ocean Engineering

journal homepage: www.elsevier.com/locate/oceaneng

Dimensional optimization of a two-body Wave energy converter using response surface methodology

Saeed Rezaei [a,*], Amir Rahimi [a], Jamshid Parvizian [a], Shahriar Mansourzadeh [b], Alexander Düster [c]

[a] Department of Mechanical Engineering, Isfahan University of Technology, Isfahan, 84156-83111, Iran
[b] Research Institute for Subsea Science & Technology, Isfahan University of Technology, Isfahan, 84156-83111, Iran
[c] Institute for Ship Structural Design and Analysis, Hamburg University of Technology (TUHH), Am Schwarzenberg Campus 4 C, D, 21073, Hamburg, Germany

ARTICLE INFO

Keywords:
Wave energy converter
Point absorber
Dimensional optimization
Response surface methodology

ABSTRACT

This paper proposes a dimensional optimization procedure for a laboratory scale two-body point absorber wave energy converter (WEC) using the design of experiment (DoE) methodology. Response surface methodology (RSM) is utilized to estimate a second order polynomial function correlating the average absorbed power, as the objective function, to five geometric parameters. Optimum values of parameters correspond to the peak of the surface fitted to the absorbed powers calculated for different sets of input parameters selected by the Box-Behnken design (BBD). The sensitivity of the objective function with respect to each parameter is investigated. The WEC is assumed to operate under regular waves in a specified range of frequency, 0.5–1 Hz. The amplitude and complex-conjugate controls are applied to keep the power take-off (PTO) system in optimum conditions. ANSYS-AQWA is used to calculate hydrodynamic parameters of the WEC required to solve the equations governing the absorbed power.

1. Introduction

Harvesting energy from sustainable resources seems to be an answer to the increasing demand for energy, with a minimum ecological footprint. Energy that is stored in oceanic waves – and released in every cycle – is one of the unlimited sustainable resources that have been in the focus of attention in recent years. In recent decades, a wide variety of technologies to harvest wave energy has been proposed, studied, and in some cases tested at full scale in real ocean conditions.

The devices that are used to generate electricity using ocean waves, generally known as wave energy converters (WECs), are classified into different categories based on their configuration and operating principle. According to Drew et al. (2009) and Falcão (2010), three main categories are oscillating water column (OWC), overtopping, and oscillating body. Among the oscillating body types, point absorbers, which were developed for the offshore environment, are rather attractive due to their simplicity and reliability compared to other designs. The horizontal dimensions of point absorber systems (PAs) are, compared to the wave length, very small. PAs consist of buoys that oscillate with incident waves in the heave or surge directions. Based on the number of oscillating bodies, PAs are grouped into single- or two-body point absorbers.

Two single-body point absorber WECs (1B-PA WEC) with different shapes of buoys are studied in Pastor and Liu (2014). By comparing a variety of diameters and drafts (the wet height of the buoy), the optimal draft, and diameter of the buoy that maximize the power absorption are determined. It is concluded that increasing the diameter of the buoy leads to an increase in the absorbed power, while the shape does not have a considerable effect.

One way to increase the output power of a WEC is to ensure that the natural frequency of the WEC is close to the frequency of the ocean waves. In other words, the WEC should operate near its resonance condition. The frequency range of the ocean waves depends on the sea states. The lowest frequency for wind-induced gravity waves is estimated to be approximately 0.03 Hz, and the highest frequency is approximately 13.6 Hz (Massel, 2007). Therefore, the diameter and the mass of the buoys should be large enough to ensure that the frequency of the WEC body falls into this range. Incorporating a submerged body, in order to improve resonance conditions, increases the degrees of freedom and, therefore, reduces the resonating frequency and increases the

* Corresponding author.
E-mail address: rezaei.sr@me.iut.ac.ir (S. Rezaei).

https://doi.org/10.1016/j.oceaneng.2022.112186
Received 24 April 2022; Received in revised form 20 June 2022; Accepted 31 July 2022
Available online 12 August 2022

absorbed power at lower frequencies (Engström et al., 2011; Liang and Zuo, 2017). Due to this fact, there is still ongoing research concerning two-body Point Absorber WECs (2B-PA WECs). This kind of WECs, in general, has three main parts: (i) the floating buoy, which is in touch and oscillates with the incident wave, (ii) the submerged body, which is immersed in the water and moves with respect to the floating body, and (iii) the power take-off system (PTO), which is placed between the two bodies and is responsible for converting the absorbed wave energy into electricity. The floating buoy and the submerged body are free to move relative to each other, in heave direction. This relative motion is converted to electricity through the PTO.

Increasing the efficiency of WECs is still the focus of ongoing research (Golbaz et al., 2021). Unpredictable wave conditions and the multidisciplinary nature of the structure of WECs are still main challenges in the development of WECs (Falcão, 2010; Falnes and Kurniawan, 2020; Al Shami et al., 2019a,b). Efforts made so far to design and improve WECs can be divided into four main lines of research: (i) to optimize the *geometry* and the *size of the buoys* in order to maximize the power absorption (Mccabe, 2013; Koh et al., 2015; Kurniawan and Moan, 2012; Goggins and Finnegan, 2014); (ii) to find the PTO proper parameters and a suitable structure to optimize the performance of the energy conversion (López et al., 2017; Gaspar et al., 2018; Boren et al., 2016), (iii) to develop control algorithms to improve the output power generation and predict the wave characteristics (Hong et al., 2014; Park et al., 2016; Murai and Sakamoto, 2021), and (iv) to design and optimize the layout of WEC farm (Sharp and Dupont, 2018; Murai et al., 2020). These lines of research are interdependent, and any effort in one line is dependent on the parameters and variables of the others. This complicates the optimization process. For example, the size and topology of the WEC's body affect the hydrodynamic coefficients and, thus, also the coefficients of the PTO and the resonance frequency.

Power absorption for two buoys of different sizes, with and without the presence of a submerged body, is studied in (Bozzi et al., 2013). The study reveals that the smaller floating buoy with a submerged body harvests 25% more power than the bigger floating buoy without a submerged body. Amiri et al. (2016) investigated the effects of wave characteristics (height and period) and the device parameters (diameter, draft, form, and PTO damping coefficient) on the efficiency of the energy conversion. They conclude that a coaxial-cylinder floating buoy shows a better performance than spherical, flat cylinder, or conical buoys.

Beatty et al. (2015) and Beatty et al. (2019) provide experimental and numerical comparisons of two typical designs of 2B-PA with two different submerged bodies: (i) Powerbuoy, developed by Ocean Power Technology (OPT) in the USA (Ocean Power Technologies, 2021) and (ii) Wavebob, developed in Ireland (Weber et al., 2009). For each design, hydrodynamic coefficients and the absorbed power are obtained. They conclude that the submerged body of Wavebob has a much higher natural frequency than Powerbuoy's submerged body – due to the combination of low buoyancy stiffness and high added mass of the damper plate of Powerbuoy. In terms of power absorption, mainly due to the very large added mass of the damper plate, Powerbuoy shows peak power absorption at much lower frequencies than Wavebob.

Adding a tuned inertia mass (TIM) significantly increases the energy absorption and broadens the effective frequency bandwidth of a novel point absorber WEC (Haraguchi and Asai, 2020). Yang et al. (2021) present an inertia self-tuning phase control strategy which can optimize the efficiency of power absorption of a multi-body WEC by modifying the natural frequency of WEC and matching it with the incident wave frequency.

For a single-body WEC, Wen et al. (2018) consider the objective function to include the maximum power absorption, bandwidth, and resonance frequency. The design of experiments (DoE) is used to optimize the draft, radius, and angle of a truncated conical WEC. They conclude that an increase in any of the three parameters decreases the resonance frequency, and increases the absorbed power. Also, an increase in the draft and/or the radius leads to a decrease in bandwidth. Drawing on the Taguchi method, Al Shami et al. (2019) capture the maximum power of a WEC operating in the Australian water regions, based on a parametric study on the performance of a 2B-PA WEC. Summarizing, they suggest the best parameter combinations to achieve maximum output power, best resonance frequency, and optimal frequency bandwidth.

Falnes (1999) develops motion equations of a 2B-PA by considering the PTO as a spring-damper system. By obtaining the optimal PTO parameters, the author estimates the maximum absorbed power. Two optimal and sub-optimal PTO designs are proposed for a 2B-PA in (Liang and Zuo, 2017), and a case study is conducted to evaluate the influence of the submerged body on the absorbed power of a two-body system, in both optimal and sub-optimal designs under regular and irregular wave excitations. Li et al. (2020) enhance the performance of a rotational PTO by proposing mechanical motion rectifiers (MMR).

The performance of a heaving coaxial-cylinder wave energy converter is optimized through the actively controlled adjustment of the damping and stiffness using a linear frequency domain model (Jin et al., 2019). The optimization process leads to an increase in the frequency bandwidth and a better "capture width ratio". The effects of water depth, mooring stiffness, and the dimensions of a WEC on the capture width ratio are studied as well. A variable-geometry wave energy converter, presented in (Zou and Abdelkhalik, 2020), employs multiple controllable panels and a gas chamber to allow the buoy to change its shape in response to changing wave conditions. In similar studies to design controllable PAs, in the case of condition control, many researches focus on latching (Babarit and Clément, 2006; Wu et al., 2018), de-clutching (Babarit et al., 2009; Zhang et al., 2014) and model predictive control (Li and Belmont, 2014; Son and Yeung, 2017; Jama et al., 2018) to keep the buoys in the same phase with the incident.

(Murai et al., 2021) present a numerical method to derive optimal control force parameters in order to maximize power absorption of a multi PA-WEC. They consider several factors such as hydrodynamic radiation and diffraction interactions and power loss in circuits to investigate different array arrangement and control force parameters. Their results reveal that optimizing array arrangement and control force parameters increase the efficiency of the power absorption by 15% and 5%, respectively.

The current paper reports the latest achievements of a project on the design and fabrication of a 2B-PA WEC. It presents a method for obtaining the optimal dimensions of the WEC, as well as the optimal parameters of the PTO, subjected to physical constraints such as wave specifications, laboratory limits such as the size of the wave tank, and fabrication costs. In the present study, a scaled-down model is optimized and tested in a wave tank. Using the dimensional analysis, *i.e.* Froude similarity in this case, the results can be generalized for models of any scales. Table 1 compares several studies performed with the aim of optimization of point absorber WECs.

Basically, the main configuration used is similar to Powerbuoy PB150. It operates in the period wave range of 5–12 s. The laboratory-scaled model is tested in a wave tank under regular waves. The test frequency range is 0.5–1 Hz, following the Froude similarity (Sheng et al., 2014). In this phase, the aim is to specify the buoys' dimensions in order to absorb the maximum power in the determined wave frequency range. The unknown parameters are the diameter and draft of the floating buoy, the diameter and thickness of the submerged body, and the depth of the WEC body. First, considering the dimensions of the wave tank, the feasible range of each unknown parameter is specified. Then, by employing the DoE method, several models, with dimensions within the feasible ranges, are selected for the simulations.

Using the boundary element method (BEM), hydrodynamic coefficients of each model are calculated using ANSYS-AQWA (ANSYS Inc., 2017). Simultaneously, by implementing amplitude control and complex-conjugate control methods (Falnes and Kurniawan, 2020) in motion equations, the PTO parameters are optimized. After determining the absorbed power of each model, response surface methodology (RSM)

Table 1
Comparing optimization processes used for WECs.

	Shadman et al. (2018)	Wen et al. (2018)	Al Shami et al. (2019)	Present work
Type of WEC	Single-body PA	Single-body PA	Two-body PA	Two-body PA
Input parameters	Buoy diameter	Buoy diameter	Floating buoy diameter	Floating buoy diameter
	Buoy draft	Buoy draft	Floating buoy draft	Floating buoy draft
		Buoy cone angle	Submerged body geometry	Submerged body diameter
			Submerged body volume	Submerged body depth
			Submerged body depth	Submerged plate thickness
PTO parameters	Optimized	Optimized	Fixed values	Optimized
DoE method	RSM	RSM	Taguchi	RSM
Optimal dimensions	Selected from given values	Optimized	Selected from given values	Optimized
Viscus effect	Unconsidered	Unconsidered	Considered	Considered
Validation	–	–	–	Yes

(Khuri and Mukhopadhyay, 2010) is used to define the absorbed power in terms of the aforementioned parameters, and to determine the optimal value of each dimension.

In Section 2 of this paper, the equation of motion for a 2B-PA is derived and optimal parameters of PTO and the output power are obtained. Then, in Section 3, DoE and RSM are employed to calculate the optimum dimensions of the PA considering the practical constraints. Section 4 focuses on the description of the numerical simulations that are performed to calculate the optimum power absorption. Section 6 concludes the paper.

2. Modeling

To provide a mathematical model of the WEC, the interactions between the sea waves, moving body, and PTO system should be considered. This requires the study of the dynamics and hydrodynamics of the system. Fig. 1 shows a WEC that interacts with ocean waves. As shown, the WEC tends to move and rotate in three directions. However, it is constrained to oscillate only in the heave direction. The equation of motion for this system, known as the Cummins equation (Babarit et al., 2012), is:

$$(m+A)\ddot{x}(t) = F_{HS}(t) + F_{Vis}(t) + F_{Rad}(t) + F_e(t) + F_{PTO}(t) \tag{1}$$

in which the left-hand side describes the acceleration of the WEC body accounting for its mass (m) and the added mass (A), which represents the accelerated mass of the water surrounding the WEC body. The right-hand side includes the forces acting on the PA:

- Hydrostatic force (F_{HS}),
- Viscous damping force (F_{Vis}),
- Radiation damping force (F_{Rad}),
- Wave excitation force (F_e),
- PTO Force, (F_{PTO}).

To simplify the approach, 2B-PA WEC can be modeled as a 2-DoF mass-spring-damper system. Fig. 2 represents this model. An axisymmetric conical floating buoy is placed on the water surface and attached to a cylindrical submerged body through a PTO. The PTO is also modeled as a mass-spring-damper system (m_{PTO}, the mass of PTO, contributes to the floating and submerged masses). A common approach to determine hydrodynamic forces is to use the linear wave theory. This theory assumes that waves are the sum of incident, radiated and diffracted components (Hudspeth, 2006; Stoker, 2011).

Eqs. (2) and (3) represent the system of equations of motion of 2B-PA WEC. To derive these equations, it is assumed that movement of the floating buoy does not affect the hydrodynamics coefficients of the submerged body, and vice versa.

$$(m_1 + A_1 + r\cdot m_{PTO})\ddot{x}_1(t) + (B_1 + b_{vis1})\dot{x}_1(t) + K_{s_1}x_1(t) + C_{PTO}(\dot{x}_1(t) - \dot{x}_2(t)) + K_{PTO}(x_1(t) - x_2(t)) = f_{e_1}(t) \tag{2}$$

$$(m_2 + A_2 + (1-r)m_{PTO})\ddot{x}_2(t) + (B_2 + b_{vis2})\dot{x}_2(t) + K_{s_2}x_2(t) + C_{PTO}(\dot{x}_2(t) - \dot{x}_1(t)) + K_{PTO}(x_2(t) - x_1(t)) = f_{e_2}(t) \tag{3}$$

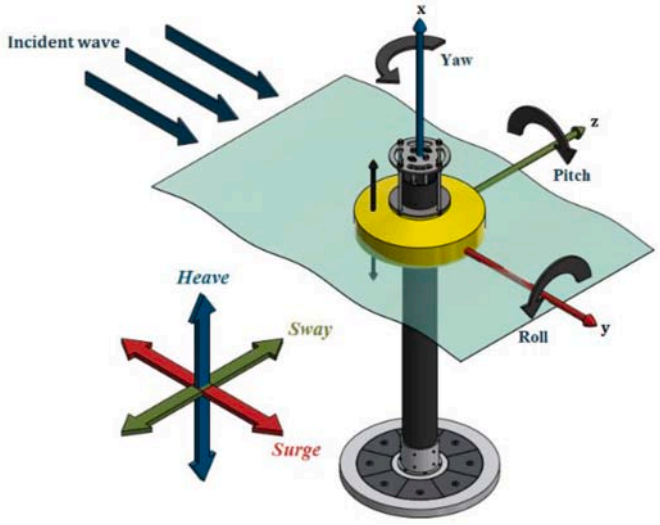

Fig. 1. Interaction of the WEC and ocean waves.

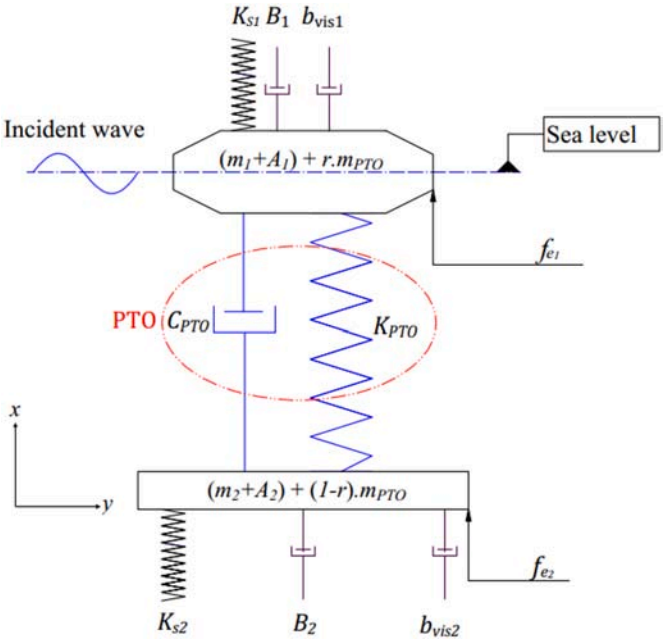

Fig. 2. A simplified model of a 2B-PA WEC in the heave direction.

To convert Eqs.*(2)* and *(3)* from time to frequency domain, we can replace $\dot{x}(t)$ and $f_e(t)$ by:

$$\dot{x}(t) = Re\{\widehat{U}e^{i\omega t}\} \tag{4}$$

$$f_e(t) = Re\{\widehat{F}_e e^{i\omega t}\} \tag{5}$$

where i is the imaginary unit, $\widehat{U}$ and $\widehat{F}$ represent the amplitudes of the velocity and force in complex notation, respectively, and $Re\{\cdot\}$ denotes the real part of a complex quantity. Accordingly $x(t)$ and $\ddot{x}(t)$ are given as Eqs. (6) and (7) respectively.

$$x(t) = Re\left\{\frac{-i}{\omega}\widehat{U}e^{i\omega t}\right\} \tag{6}$$

$$\ddot{x}(t) = Re\{i\omega\widehat{U}e^{i\omega t}\} \tag{7}$$

The matrix form of the equation of motion in the frequency domain can be written as:

$$\left(i\omega M + C - \frac{i}{\omega}K\right)\left[\widehat{U}_1\ \widehat{U}_2\right]^T = \left[\widehat{F}_{e_1}\ \widehat{F}_{e_2}\right]^T \tag{8}$$

in which M, C, and K are the matrices of mass, damping, and stiffness coefficient, respectively, defined as:

$$M = \begin{bmatrix} (m_1 + A_1) + r{\cdot}m_{PTO} & 0 \\ 0 & (m_2 + A_2) + (1-r)m_{PTO} \end{bmatrix} \tag{9}$$

$$C = \begin{bmatrix} (B_1 + b_{Vis1} + C_{PTO}) & -C_{PTO} \\ -C_{PTO} & (B_2 + b_{Vis2} + C_{PTO}) \end{bmatrix} \tag{10}$$

$$K = \begin{bmatrix} (K_{PTO} + K_{s1}) & -K_{PTO} \\ -K_{PTO} & (K_{PTO} + K_{s2}) \end{bmatrix} \tag{11}$$

where subscripts 1 and 2 refer to the parameters of the floating buoy and the submerged body, respectively. The fraction of PTO mass contributing to the floating buoy is represented by r. The added mass of each body, radiation damping, hydrostatic stiffness, and wave frequency are denoted by A, B, K_s, and ω, respectively, while b_{vis} stands for the viscous damping. The complex mechanical impedance matrix Z(ω) reads

$$Z(\omega)[\widehat{U}_1\,\widehat{U}_2]^T = \begin{bmatrix} Z_1 + Z_{PTO} & -Z_{PTO} \\ -Z_{PTO} & Z_2 + Z_{PTO} \end{bmatrix}\left[\widehat{U}_1\,\widehat{U}_2\right]^T = \left[\widehat{F}_{e_1}\,\widehat{F}_{e_2}\right]^T \tag{12}$$

where

$$Z_1 = (B_1 + b_{vis1}) + i\omega\left((m_1 + A_1) + r\cdot m_{PTO} - \frac{K_{s1}}{\omega^2}\right) \tag{13}$$

$$Z_2 = (B_2 + b_{vis2}) + i\omega\left((m_2 + A_2) + (1-r)m_{PTO} - \frac{K_{s2}}{\omega^2}\right) \tag{14}$$

$$Z_0 = Z_1 + Z_2 \tag{15}$$

and

$$Z_{PTO} = C_{PTO} + i\omega\left(-\frac{K_{PTO}}{\omega^2}\right) \tag{16}$$

Drawing on Eq. (12), the relative velocity of the two bodies can be given as:

$$\widehat{U}_{rel} = \widehat{U}_1 - \widehat{U}_2 = \frac{\frac{\widehat{F}_{e1}Z_2}{(Z_1+Z_2)} - \frac{\widehat{F}_{e2}Z_1}{(Z_1+Z_2)}}{\frac{Z_1Z_2}{(Z_1+Z_2)} + Z_{PTO}} \tag{17}$$

By defining the equivalent wave excitation force ($\widehat{F}_0$) and the equivalent complex mechanical impedance (Z_{eq}), the relative velocity of bodies, Eq. (17), can be rewritten as:

$$\widehat{U}_{rel} = \frac{\widehat{F}_0}{Z_{eq} + Z_{PTO}} \tag{18}$$

in which:

$$Z_{eq} = \frac{Z_1Z_2}{Z_0} \tag{19}$$

$$\widehat{F}_0 = \frac{\widehat{F}_{e1}Z_2 - \widehat{F}_{e2}Z_1}{Z_0} \tag{20}$$

Therefore, the time-averaged value of mechanical absorbed power, $\overline{p_u(t)}$, can be determined by multiplying the PTO force by the relative velocity of the two bodies (Falnes, 1999):

$$P_u \equiv \overline{p_u(t)} = \overline{f_{PTO}(t)\cdot u_{rel}(t)} = \frac{1}{2}C_{PTO}|\widehat{U}_{rel}|^2 \tag{21}$$

$$P_u = \frac{1}{2}C_{PTO}\left|\frac{\widehat{F}_0}{(C_{PTO} + Re\{Z_{eq}\}) + i\left(Im\{Z_{eq}\} - \frac{K_{PTO}}{\omega}\right)}\right|^2 \tag{22}$$

For a specific WEC geometry, the parameters of Z_{PTO}, i.e. K_{PTO} and C_{PTO}, can be adjusted to achieve the maximum power.

To extract the maximum time-averaged mechanical absorbed power, two approaches can be followed. The first approach aims to minimize the denominator of Eq. (22) by dismissing the imaginary part given in Eq. (23). This ensures that the exciting wave force and the relative velocity of two bodies act in phase and results in the optimum stiffness of the PTO, Eq. (24). This approach is known as *complex-conjugate control*.

$$Im\{Z_{eq}\} - \frac{K_{PTO}}{\omega} = 0 \tag{23}$$

$$K_{PTO_{opt}} = \omega Im\{Z_{eq}\} \tag{24}$$

If (at a certain wave frequency) a negative value is obtained for K_{PTO}, its magnitude is considered to be zero. In this case, a suboptimal value is obtained for the power, since a negative spring coefficient is not practically meaningful:

$$K_{PTO_{subopt}} = 0 \tag{25}$$

The second approach, known as *amplitude control*, utilizes the partial derivative (Appendix A) to maximize the mechanical absorbed power as:

$$\frac{\partial P_u}{\partial C_{PTO}} = 0 \tag{26}$$

Thus, the optimum damping of the PTO is achieved:

$$C_{PTO_{opt}} = \sqrt{\left(Re\{Z_{eq}\}\right)^2 + \left(Im\{Z_{eq}\} - \frac{K_{PTO}}{\omega}\right)^2} \tag{27}$$

The maximum time-averaged power can be captured by applying both control methods simultaneously. Thus, based on the value of the PTO stiffness, the optimum power is derived as (Falnes, 1999):

$$P_{u_{opt}} = \frac{|\widehat{F}_0|^2}{8Re\{Z_{eq}\}} \tag{28}$$

For the suboptimal case,

$$P_{u_{subopt}} = \frac{|\widehat{F}_0|^2}{4\left(Re\{Z_{eq}\} + |Z_{eq}|\right)} \tag{29}$$

3. Optimizing the WEC geometry using optimum PTO parameters

The previous section demonstrated a major step in maximizing the absorbed power by optimizing the PTO parameters. We can also opti-

mize the dimensions of the WEC to further increase the absorbed power. Using complex-conjugate and amplitude controls, the optimal values of the PTO parameters can be determined using Eqs. (24) and (27). To specify the dimensions, all the constraints should be taken into account, and the impact of each should be considered. There are five major dimensional parameters, shown in Fig. 3, which play important roles in defining the geometry of a new 2B-PAWEC: the floating buoy diameter (D_1) and its weight, which is directly related to the draft (H_d), the submerged body heave plate diameter (D_2) and its thickness (t), and the height (depth) of the submerged body (H).

The WEC is planned to be constructed and tested in a wave tank. Therefore, all physical constraints must also come into consideration. The dimensions of the WEC might be bounded by various factors, such as fabrication cost and capacity, operation conditions, etc. In the current study, one constraint arises from the dimensions of the available wave tank, i.e. its width and height, in which the WEC prototype is going to be tested. In order to minimize disturbances in the experimental results, the prototype should be small enough to minimize the effect of wave reflections from the walls and bottom of the wave tank. Thus, the diameter of the oscillating buoys needs to be at least five times smaller than the width of the wave tank (Chakrabarti, 1999; Payne et al., 2009).

On the other hand, the diameter of the WEC should be large enough to guarantee a turbulence flow. This facilitates a 'scale up' of the results for industrial size WECs operating in the sea.

The movement of each body may affect the hydrodynamic characteristics of the other. To minimize this likely negative effect, the distance between the two bodies should be adequately large. On the other hand, to avoid reflections from the bottom surface of the wave tank, the submerged body should be far enough from the bottom. This imposes a limit on the distance between the two bodies of the WEC.

The draft of the floating buoy, i.e. the wet height of the buoy, and the diameter of the buoy determine the buoyancy force; this force should be balanced by the weight of the buoy. The weight of each buoy is limited by fabrication contraints and material density. Theoretically, there is no upper bound for the draft of the floating buoy and the thickness of the heave plate – so any practical range can be assumed. By taking all constraints and assumptions into account, the dimensional ranges of the five parameters are determined, Table 2.

From among the infinite combinations of dimensional values for the WEC within the ranges provided in Table 2, the optimum values to maximize the extracted power of the WEC are chosen using DoE

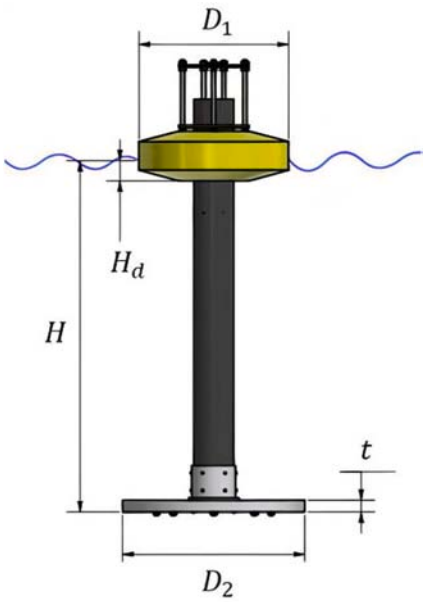

Fig. 3. 2B-PA WEC schematic.

Table 2
Dimensional ranges of WEC parameters.

Parameter	Min. (mm)	Max. (mm)
D_1	500	600
H_d	70	80
H	1200	1400
D_2	600	800
t	30	80

methods. The type of DoE used here is RSM: a statistical parametric method that provides an estimated relationship between several input variables and one or more response variables, helping to better understand and optimize the response. This method (introduced in (Khuri and Mukhopadhyay, 2010)) is appropriate where the optimum operational conditions depend on various correlated inputs.

The experimental designs for the RSM are provided by Box–Behnken Designs (BBD), allowing for a sequential study of the effect of the various factors of the design, during the study of one factor, while other factors are maintained at a constant level. For a system with five continuous parameters, BBD proposes 46 WEC models combining predetermined dimensions, see Appendix B. Every single one of the 46 generated WEC models is simulated in ANSYS-AQWA after its CAD model is built. The hydrodynamic coefficients of each model are calculated in ANSYS-AQWA. Having calculated the hydrodynamics coefficients, the maximum frequency-averaged absorbed power for each combination can be determined, for the frequency domain of 0.5–1 Hz, in MATLAB. The overall process of optimization is shown in Fig. 4.

Every experiment includes calculating the normalized frequency-averaged power for a combination of five parameters. The average is taken over the wave frequency range of 0.5–1 Hz (the frequency step is 0.1 Hz). In order to make the absorbed power independent of wave amplitude (η), it is normalized to η^2.

Once the simulation for each model is performed and the frequency-averaged absorbed power of each WEC is determined, RSM fits a parametric model (second-order polynomial) on the outcomes of the simulation in order to calculate the normalized frequency-averaged power as a function of five unknown parameters:

$$\begin{aligned} P_{Norm} = \frac{P}{\eta^2} = & -1418 + 3D_1 + 3.23D_2 + 0.65H - 13.2H_d - 0.99t \\ & - 0.01074D_1^2 - 0.007465D_2^2 - 0.000624H^2 + 0.062{H_d}^2 \\ & - 0.0056t^2 + 0.01206D_1D_2 + 0.00311D_1H - 0.0207D_1H_d \\ & + 0.01412D_1t - 0.00024D_2H + 0.0185D_2H_d - 0.01153D_2t \\ & - 0.0025H{\cdot}H_d + 0.00008H{\cdot}t + 0.0194H_d{\cdot}t \end{aligned} \tag{30}$$

This model establishes a relationship between the average power absorbed by the WEC and its dimensions. To evaluate the model, several measures are to be checked. First, to determine how well the model fits the data, the percentage of variation in the response that is explained by the model is represented by R^2. If the model fits well, R^2 is close to 1. for the current model, R^2 is 0.9926. R^2 also shows that skipping parameters with a degree higher than 2 has little effect on the output.

To determine the effect of each parameter on the output, the analysis of variance (ANOVA) (St and Wold, 1989) is used. The results, using Minitab (Ryan et al., 2012), are presented in Table 3, in which:

- DF (degree of freedom) represents the number of parameters that appear in the equation; the model consists of 5 linear terms, 5 quadratic terms, and 10 two-way interaction terms.
- Adjusted sums of squares (Adj. SS) are measures of variation for different terms of the model, while adjusted mean squares (Adj. MS) measure how much variation a term or a model explains – assuming that all other terms are in the model, regardless of the order they were entered. Adj. SS and Adj. MS are used to calculate the P-value

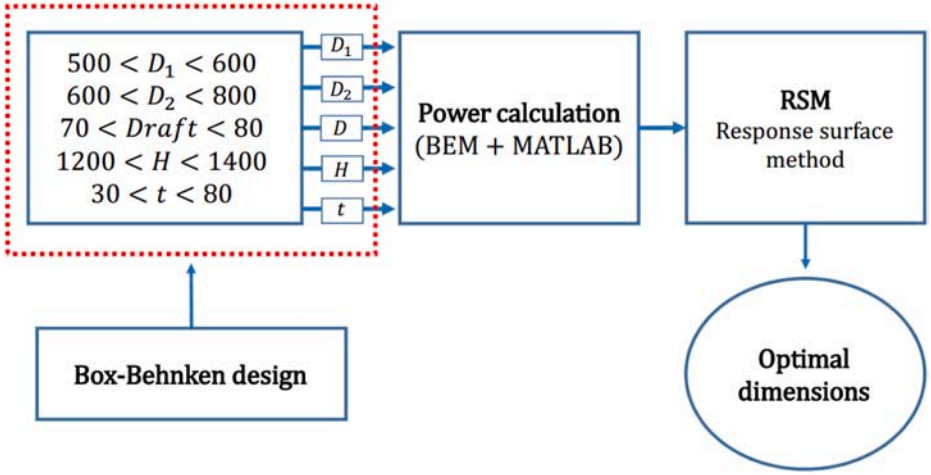

Fig. 4. Optimization process.

Table 3
ANOVA data for the model. DF: degree of freedom; Adj. SS: adjusted sum of squares; Adj. MS: adjusted mean squares.

Source	DF	Adj. SS	Adj. MS	F-value	P-value
Model	20	449235	22462	166.92	0.000
Linear	5	371359	74272	551.94	0.000
D_1	1	334933	334933	2489.01	0.000
D_2	1	3336	3336	24.79	0.000
H	1	23493	23493	174.59	0.000
H_d	1	8327	8327	61.88	0.000
t	1	1271	1271	9.44	0.005
Square	5	57290	11458	85.15	0.000
D_1^2	1	6296	6296	46.79	0.000
D_2^2	1	48590	48590	361.09	0.000
H^2	1	340	340	2.52	0.125
${H_d}^2$	1	21	21	0.16	0.696
t^2	1	107	107	0.79	0.382
Two-way interaction	10	20586	2059	15.30	0.000
D_1D_2	1	14549	14549	108.12	0.000
D_1H	1	967	967	7.19	0.013
D_1H_d	1	107	107	0.80	0.381
D_1t	1	1246	1246	9.26	0.005
D_2H	1	23	23	0.17	0.683
D_2H_d	1	340	340	2.53	0.124
D_2t	1	3324	3324	24.70	0.000
$H\cdot H_d$	1	7	7	0.05	0.828
$H\cdot t$	1	0	0	0.00	0.973
$H_d\cdot t$	1	24	24	0.17	0.679

for a term and also to calculate the R^2 statistic. Usually, when in interpreting a model, it is more common to use the P-values and the R^2 statistic than the sums of squares.

- The F-value is a statistical test used to determine whether each factor is associated with the response or not (St and Wold, 1989). The larger the F-value, the more the response depends on that parameter. A sufficiently large F-value indicates that the term or model is significant. The F-value is also used to calculate the P-value.
- The P-value is a probability measure used to make a decision about the statistical significance of the terms and model. If the P-value is less than or equal to the significance level, e.g. 0.05 (Neter et al., 1996), then the effect of the term is statistically significant

To depict the data provided in Table 3, a Pareto chart is used for the standardized values of the parameters, Fig. 5. For the calculation procedure of the standardized values, the reader is referred to (Wilkinson, 2006). The red dashed line shows the standard value corresponding to the P-value of 0.05. As mentioned, any term with a P-value larger than 0.05 does not have a major impact on the output power – and can thus be ignored.

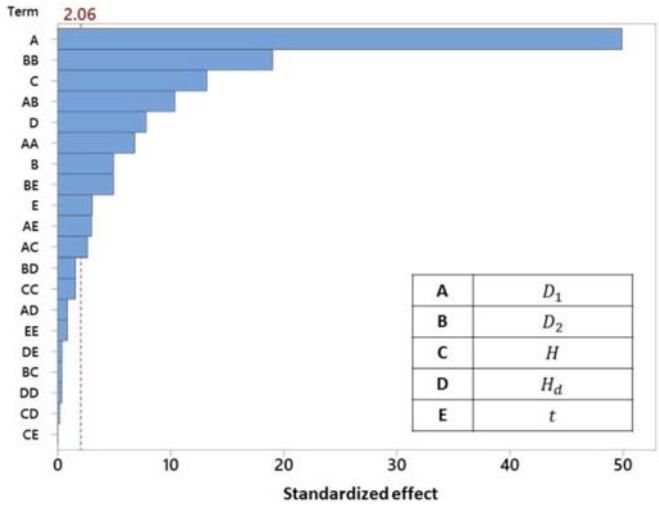

Fig. 5. Pareto chart for the normalized absorbed power. A: the floating buoy diameter (D_1); B: the submerged body diameter (D_2); C: the distance between floating and submerged bodies (H); D: the draft (H_d); E: the submerged body thickness (t).

Fig. 6 illustrates how the variation of the output power depends on the variation of each of the input parameters at the peak of the RSM fitted surface. It shows that increasing parameters such as floating buoy diameter and the depth of the submerged body has a positive effect on the power. On the other hand, as the figure shows, increasing the draft has a negative impact on the absorbed power. In other words, the lower the weight of the floating body, the greater the absorbed power. However, the lower bound of the weight of the buoy is limited by fabrication constraints.

As the figure indicates, increasing the diameter of the submerged body initially increases the output power; however, after passing a certain value, the absorbed power decreases with a further increase in diameter. Therefore, there is an optimum value for the submerged body diameter in the defined range, within the selected wave frequency range.

Fig. 7 depicts the optimum value of each dimension, obtained from the current RSM, within the selected range of wave frequency. Substituting the optimum dimensions into Eq. (30), the maximum frequency-averaged absorbed power can be calculated to be 1453 W/m^2. It should be noted that the power is normalized with respect to the

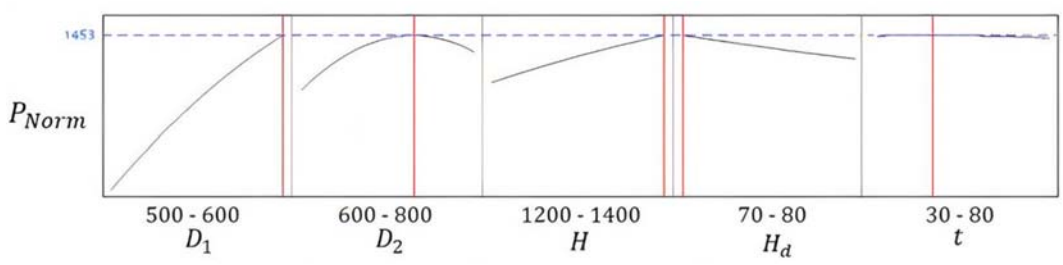

Fig. 6. The impact of different parameters on the averaged absorbed power.

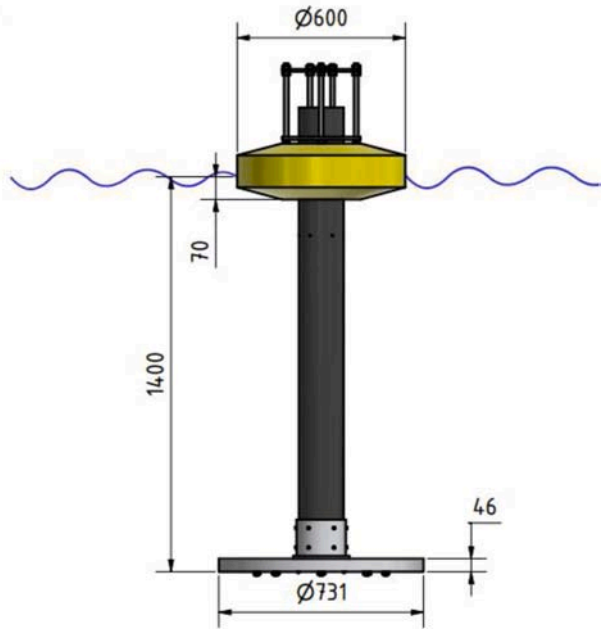

Fig. 7. Optimal dimensions of the WEC.

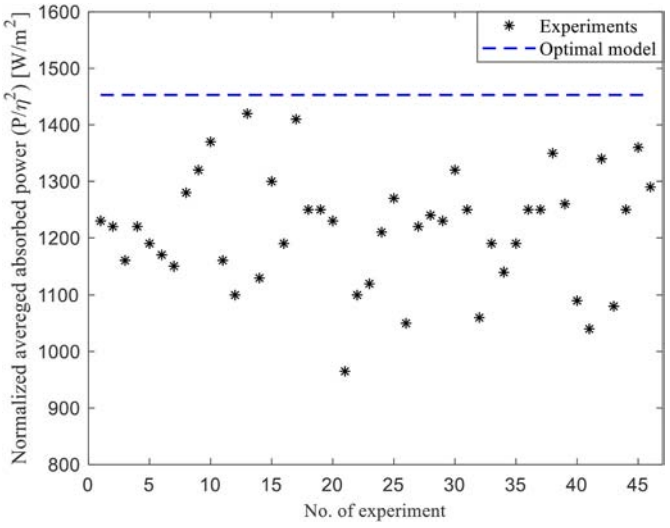

Fig. 8. The normalized frequency-absorbed power for DoE cases. The dashed line indicates the frequency-averaged absorbed power for the optimal model.

wave amplitude. The estimated maximum normalized frequency-averaged power as well as the normalized frequency-averaged power of all 46 cases are shown in Fig. 8.

As it turned out, the diameters of floating and submerged buoys are important parameters that affect the output power. Fig. 9 shows how the power changes with respect to the diameter of two bodies by keeping the other three parameters constant in the optimal amount. Each contour represents 100 units of power change. By comparing the ratio of the height to the width of each contour, the effect of the floating buoy diameter on the absorbed power is determined with respect to the diameter of the submerged body. For example, by selecting a floating buoy diameter of 600 mm, for any diameter of the submerged body in the range of 650–800 mm, the power is always above 1400 W/m^2.

Since the maximum normalized frequency-averaged power is obtained by finding the peak of the RSM fitted surface on the normalized frequency-averaged powers of the selected set of input parameters, it is only an estimate of the maximum power. Dimensions corresponding to the estimated maximum power obtained by RSM are now used in ANSYS-AQWA to calculate the hydrodynamic coefficients. Then, Eq. *(29)* can be used to determine the exact averaged optimum power. To show how the BEM is used to calculate the normalized averaged power during the optimization process, the details of the calculations of the hydrodynamic coefficients for the optimum WEC dimensions are given in detail in Section 4.

4. Hydrodynamic coefficients and the output power

ANSYS-AQWA is used to calculate the hydrodynamics coefficients, including the added mass coefficients A_1 and A_2, damping coefficients B_1 and B_2, and excitation forces $\widehat{F}_{e1}$ and $\widehat{F}_{e2}$ of the floating buoy and submerged body, respectively. These coefficients appear in Eq. *(12)*. Fig. 10 shows the mesh used to simulate the optimized WEC dimensions by ANSYS-AQWA.

The resulting added mass obtained for the floating and submerged bodies of the WEC, for the frequency range of 0.2–1 Hz, is shown in Fig. 11. Note that only the results obtained for the frequency range of 0.5-1 Hz will be used for optimization purposes. As shown in this figure, the added mass of the submerged body is at least three times larger than that of the floating body, within the specified wave frequency range. Also, as expected, the added mass of the submerged body is a weak function of the wave frequency, while the added mass of the floating buoy changes noticeably with the wave frequency, especially within the frequency range 0.5–1 Hz.

Fig. 12 represents the results obtained for the radiation damping coefficients of the floating and submerged bodies. As shown, the radiation damping coefficient of the floating body is much larger than that of the submerged body, which is due to its large surface contact with the free water. Since ANSYS-AQWA essentially deals with the inviscid flow, it does not consider the effect of viscosity or frictional drag when calculating the damping coefficient. This does not have any significant effect on the damping coefficient of the floating buoy (Beatty et al., 2015); however, it affects the resulting damping coefficient of the submerged body. To consider the effect of viscosity, in the current study, the correlation suggested by (Liang and Zuo, 2017) is used for the submerged body:

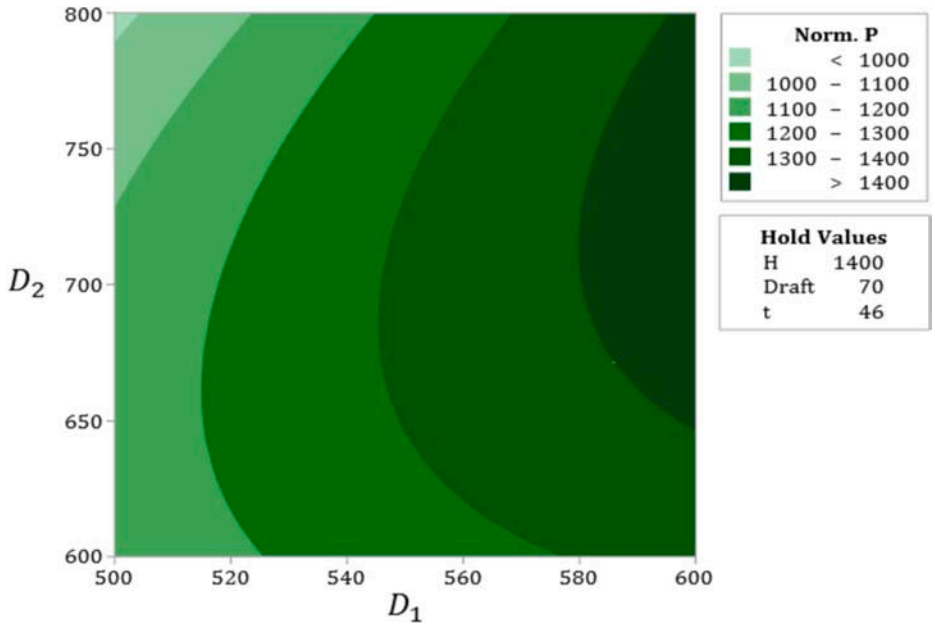

Fig. 9. Contour plot of normalized frequency-averaged absorbed power vs. the diameter of floating buoy and submerged body.

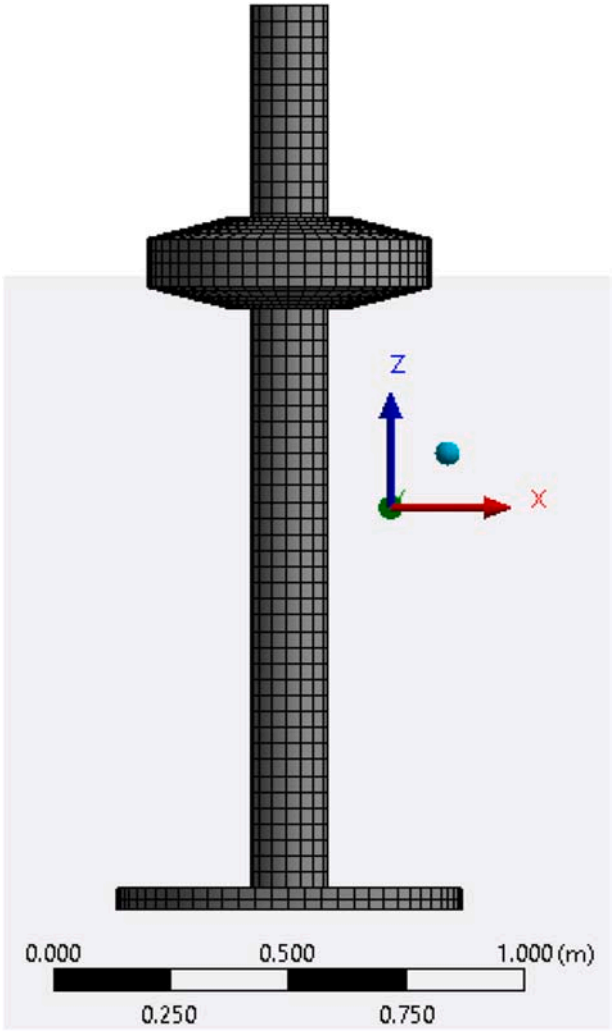

Fig. 10. The model used in BEM analyses.

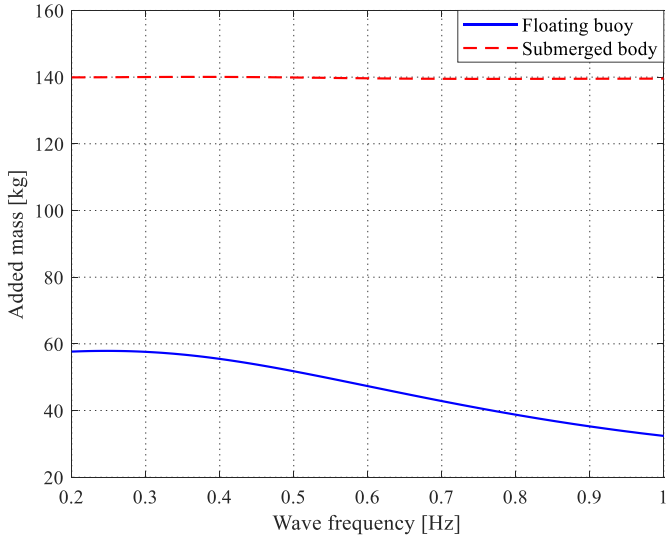

Fig. 11. Added mass coefficients of floating buoy and submerged body.

$$\zeta_2 = \frac{b_{vis_2}}{2m_1\omega_f} \tag{31}$$

where ζ_2 is the dimensionless viscous damping of the submerged body, b_{vis_2} is the viscous damping coefficient of the submerged body, m_1 is the mass of the floating buoy, and $\omega_f = \sqrt{k_{s1}/(m_1 + A_1)}$ is the natural frequency of the floating buoy in still water.

According to experimental results (Beatty et al., 2015), ζ_2 is in the range of 0.4–0.8 for the submerged body of Powerbuoy. In this research, ζ_2 is taken to be 0.6 to estimate the viscous damping coefficient of the submerged body.

Fig. 13 shows the resulting wave excitation force acting on the floating and submerged bodies, for the frequency range 0.2–1 Hz. As expected, the force acting on the floating buoy is much larger than that of the submerged body. This is due to the exponential attenuation of the wave effect with the depth of water. The figure also shows that the floating body excitation force decreases as the wave frequency increases. This is in agreement with the Haskind's equation (Falnes and

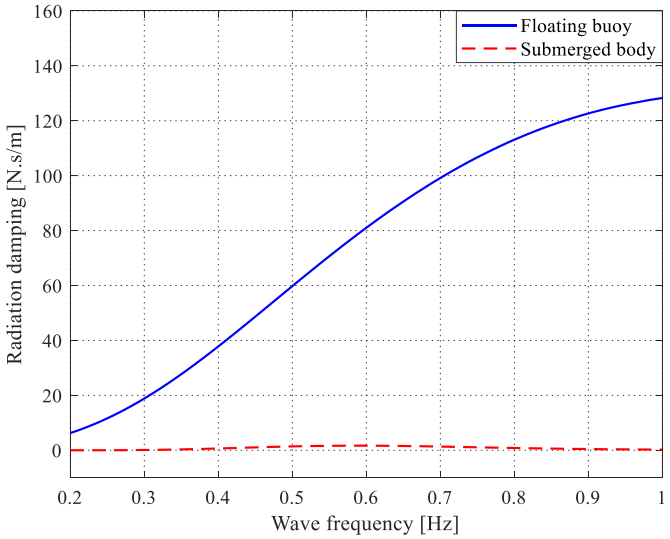

Fig. 12. Radiation damping coefficients of floating buoy and submerged body.

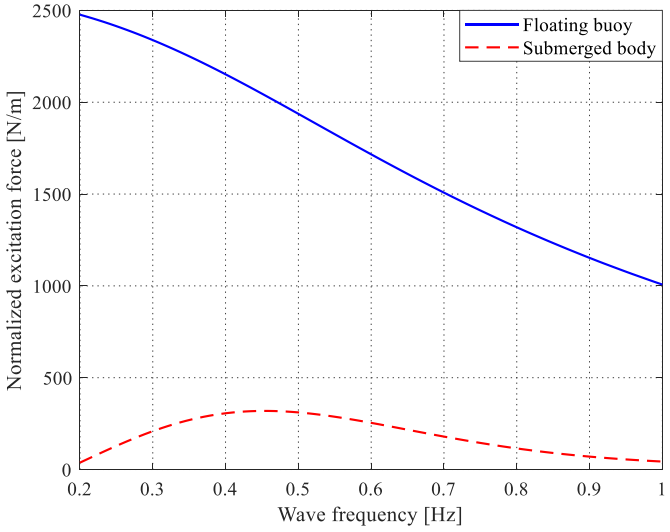

Fig. 13. The normalized excitation force amplitude acting on the floating buoy and submerged body.

Kurniawan, 2020):

$$F_e = \sqrt{\frac{2\rho g^3 B_i}{\omega^3}} \tag{32}$$

Once the hydrodynamic coefficients are calculated, Eq. *(29)* is used to determine the optimum time-averaged absorbed power. Fig. 14 shows the resulting normalized time-averaged absorbed power, as a function of the wave frequency, for the optimum dimensions of the WEC. As the figure shows, the maximum time-averaged absorbed power, 2000 W/m^2 , occurs at the frequency 0.55 Hz.

The operating frequency range of the WEC is within 0.5–1 Hz. To make it possible to compare the output powers of the WECs with various dimensions, it is assumed that during a specific period of time, each wave frequency has the same probability of occurring. Therefore, one can take the frequency-averaged of the power over the wave frequency range (0.5–1) Hz and compare the result with the corresponding values of other WECs; or one could multiply the obtained power by the probability density function of the wave frequency occurrence. The results of the numerical methods show that the value of the frequency-averaged absorbed power of the optimal WEC, in the selected frequency range,

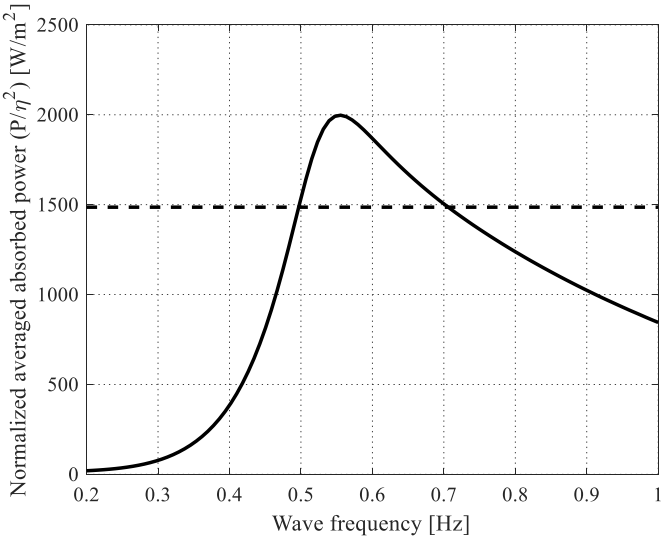

Fig. 14. The normalized averaged absorbed power.

is 1486 W/m^2. This is comparable with 1453 W/m^2, from the RSM obtained in Section 3.

The incident wave power (power flux) which is normalized to the wave amplitude, η^2, is expressed as (Falnes and Kurniawan, 2020):

$$P_{w,Norm.} = \frac{\rho g^2}{8\pi} T\left(1 + \frac{2kd}{sinh(2kd)}\right) tanh(kd) \times D \tag{33}$$

where ρ, is the density of water and g is gravity acceleration. T, k, and d are the wave period, wave number and depth of water, respectively. D is the incident wave width. The mechanical efficiency of the WEC can be assessed as:

$$eff_m = \frac{P_{Norm}}{P_{wN}} \tag{34}$$

According to RSM results, the diameter of the floating body has the most important effect on the averaged mechanical absorbed power. On the other hand, the excitation force of the floating body is several times greater than the excitation force of the submerged body, Fig. 14. Therefore in Eq. (33), D is considered as the diameter of the floating body. By averaging the normalized incident wave power upon the frequency range of 0.5–1 Hz, the mechanical efficiency of the optimized 2B-PA is calculated to be 47.5%.

5. Validation

Once the optimal WEC dimensions are specified, the model is fabricated and tested in a wave tank. Fig. 15 shows the model made with the dimensions obtained in this paper as illustrated in Fig. 7. Various experiments have been carried out to calculate the hydrodynamic coefficients of the WEC model and the absorbed power, which are discussed in details in another paper prepared by the current authors and will appear soon (Rahimi et al. Unpublished results). All the tests are performed under the regular waves. The absorbed power measured by the experiment is shown in solid black line in Fig. 16, and the black dashed line depicts the average power taken in the frequency range of 0.5–1 Hz. The blue solid and dashed lines shows the absorbed power calculated based on the hydrodynamic coefficients obtained by the ANSYS AQWA and their frequency-averaged value, respectively. The frequency-averaged absorbed power obtained by the RSM is also shown in dashed red line. As discussed in Section 4, the value that RSM proposes for optimal absorbed power is consistent with the ANSYS AQWA results. It can be seen from Fig. 16 that there is a difference between the experiment and RSM results. The discrepancy in the results is due to

Fig. 15. Fabricated WEC

viscous damping coefficients. In the optimization process, Eq. (31) is used to estimate the viscous damping, while in the experiment the exact value of the viscosity is applied.

6. Conclusions

The focus of this paper is to optimize the dimensions of a 2B-PA WEC in the laboratory scale, in order to absorb the maximum average mechanical power in a specified frequency range. The BBD is used to select 46 cases within the allowable range of dimensions. The average normalized power is calculated at each optimum control condition. ANSYS-AQWA is employed to calculate the hydrodynamic coefficients necessary to calculate the average normalized power of each setting of WEC dimensions. RSM is employed to build a second-order polynomial parametric model that fits a surface on the output powers of 46 WECs, with various dimensions. The optimum normalized average power is

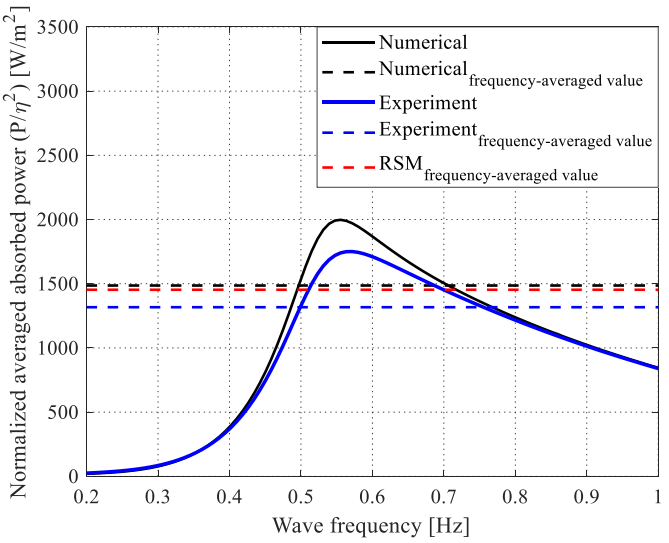

Fig. 16. Normalized absorbed power.

then estimated to be 1453 W/m^2 at the peak of the fitted surface. The exact calculation of the frequency range normalized averaged power for optimum dimensions gives a power of 1486 W/m^2, which fits well with the RSM results. The consistency of the results of the model proposed by RSM and the simulation for the optimal WEC confirms the accuracy of the RSM results.

Optimization results showed that, in the specified range of wave frequency, increasing the diameter of the floating buoy has the greatest impact on increasing the resulting absorbed energy, i.e. the output power. The second most effective parameter with regard to the absorbed energy is the diameter of the submerged body. As the diameter of the submerged body increases, the absorbed energy increases to its maximum value – however followed by a decrease in the energy if the diameter is increased even further. The depth of the submerged body, draft, and the thickness of the lower plate are next in the line of importance in increasing energy absorption. The results of ANOVA reveal that the five main variables selected have considerable effect in determining the output power, and none of them can be ignored. The results show that the optimized WEC is able to harvest 47.5% of incident wave power. The report on the fabrication and laboratory testing of an optimized WEC will be published shortly in upcoming papers.

CRediT authorship contribution statement

Saeed Rezaei: Conceptualization, Methodology, Software, Validation, Writing – original draft. **Amir Rahimi:** Conceptualization, Investigation, Visualization, Validation, Writing – original draft. **Jamshid Parvizian:** Project administration, Writing – review & editing, Funding acquisition. **Shahriar Mansourzadeh:** Supervision, Writing – review & editing, Validation. **Alexander Düster:** Project administration, Writing – review & editing, Funding acquisition.

Declaration of competing interest

The authors declare that they have no known competing financial interests or personal relationships that could have appeared to influence the work reported in this paper.

Data availability

Data will be made available on request.

Acknowledgment

The authors would like to sincerely thank the Alexander von Humboldt foundation for providing the financial support of this research.

Appendix A

The process of finding the optimal and suboptimal PTO damping coefficients using the partial derivative method (Eqs. *(26)* and *(27)*) is as follows:

$$P_u = \frac{1}{2} C_{PTO} \left| \frac{\widehat{F}_0}{\left(C_{PTO} + Re\{Z_{eq}\}\right) + i\left(Im\{Z_{eq}\} - \frac{K_{PTO}}{\omega}\right)} \right|^2 \tag{A.1}$$

$$P_u = \frac{1}{2} C_{PTO} \frac{|\widehat{F}_0|^2}{\alpha^2 + \beta^2} \tag{A.2}$$

where. $\alpha = C_{PTO} + Re\{Z_{eq}\}$

and $\beta = Im\{Z_{eq}\} - \frac{K_{PTO}}{\omega}$

$$\frac{\partial P_u}{\partial C_{PTO}} = \frac{1}{2} \frac{|\widehat{F}_0|^2}{\alpha^2 + \beta^2} \left[1 - \frac{2\alpha C_{PTO}}{\alpha^2 + \beta^2}\right] = 0 \tag{A.3}$$

Eq. (A.3) *is fulfilled when* $2\alpha C_{PTO} = \alpha^2 + \beta^2$. *Therefore, the optimal PTO damping coefficient can be given as:*

$$C_{PTO\,opt} = \sqrt{\left(Re\{Z_{eq}\}\right)^2 + \left(Im\{Z_{eq}\} - \frac{K_{PTO}}{\omega}\right)^2} \tag{A.4}$$

For the optimal values of $K_{PTO} (K_{PTO} > 0)$*:*

$$C_{PTO\,opt} = Re\{Z_{eq}\} \tag{A.5}$$

And for the suboptimal values of $K_{PTO} (K_{PTO} = 0)$*:*

$$C_{PTO\,subopt} = \sqrt{\left(Re\{Z_{eq}\}\right)^2 + \left(Im\{Z_{eq}\}\right)^2} = |Z_{eq}| \tag{A.6}$$

Appendix B

Table B.1
Experiments suggested based on Box-Behnken design

No. of experiment	D_1 [mm]	H_d [mm]	D_2 [mm]	H [mm]	t [mm]	Normalize averaged power (W/m2)
1	550	75	600	1400	55	1.23E+03
2	550	75	700	1200	30	1.22E+03
3	550	80	600	1300	55	1.16E+03
4	550	70	600	1300	55	1.22E+03
5	550	80	700	1200	55	1.19E+03
6	550	70	800	1300	55	1.17E+03
7	550	75	600	1200	55	1.15E+03
8	550	75	700	1400	80	1.28E+03
9	600	75	700	1200	55	1.32E+03
10	600	75	700	1300	80	1.37E+03
11	550	75	600	1300	30	1.16E+03
12	500	75	700	1300	30	1.10E+03
13	600	75	700	1400	55	1.42E+03
14	550	75	800	1300	80	1.13E+03
15	550	75	700	1400	30	1.30E+03
16	550	75	800	1300	30	1.19E+03
17	600	70	700	1300	55	1.41E+03
18	550	75	700	1300	55	1.25E+03
19	550	75	700	1300	55	1.25E+03
20	550	70	700	1200	55	1.23E+03
21	500	75	800	1300	55	9.65E+02
22	500	75	600	1300	55	1.10E+03
23	550	75	800	1200	55	1.12E+03
24	550	75	600	1300	80	1.21E+03
25	550	80	700	1400	55	1.27E+03
26	500	75	700	1300	80	1.05E+03
27	550	80	700	1300	80	1.22E+03
28	550	80	700	1300	30	1.24E+03
29	600	75	600	1300	55	1.23E+03

(*continued on next page*)

Table B.1 (*continued*)

No. of experiment	D_1 [mm]	H_d [mm]	D_2 [mm]	H [mm]	t [mm]	Normalize averaged power (W/m2)
30	550	70	700	1400	55	1.32E+03
31	550	75	700	1300	55	1.25E+03
32	500	80	700	1300	55	1.06E+03
33	550	75	800	1400	55	1.19E+03
34	550	80	800	1300	55	1.14E+03
35	550	75	700	1200	80	1.19E+03
36	550	75	700	1300	55	1.25E+03
37	550	75	700	1300	55	1.25E+03
38	600	80	700	1300	55	1.35E+03
39	550	70	700	1300	80	1.26E+03
40	500	70	700	1300	55	1.09E+03
41	500	75	700	1200	55	1.04E+03
42	600	75	800	1300	55	1.34E+03
43	500	75	700	1400	55	1.08E+03
44	550	75	700	1300	55	1.25E+03
45	600	75	700	1300	30	1.36E+03
46	550	70	700	1300	30	1.29E+03

References

Al Shami, E., Wang, X., Zhang, R., Zuo, L., 2019a. A parameter study and optimization of two body wave energy converters. Renew. Energy 131, 1–13.

Al Shami, E., Zhang, R., Wang, X., 2019b. Point absorber wave energy harvesters: a review of recent developments. Energies 12, 47.

Amiri, A., Panahi, R., Radfar, S., 2016. Parametric study of two-body floating-point wave absorber. J. Mar. Sci. Appl. 15, 41–49.

ANSYS, 2017. Inc. *AQWA Theory Manual*. Canonsburg, PA, vol. 15317.

Babarit, A., Clément, A.H., 2006. Optimal latching control of a wave energy device in regular and irregular waves. Appl. Ocean Res. 28, 77–91.

Babarit, A., Guglielmi, M., Clément, A.H., 2009. Declutching control of a wave energy converter. Ocean. Eng. 36, 1015–1024.

Babarit, A., Hals, J., Muliawan, M.J., Kurniawan, A., Moan, T., Krokstad, J., 2012. Numerical benchmarking study of a selection of wave energy converters. Renew. Energy 41, 44–63.

Beatty, S.J., Hall, M., Buckham, B.J., Wild, P., Bocking, B., 2015. Experimental and numerical comparisons of self-reacting point absorber wave energy converters in regular waves. Ocean. Eng. 104, 370–386.

Beatty, S.J., Bocking, B., Bubbar, K., Buckham, B.J., Wild, P., 2019. Experimental and numerical comparisons of self-reacting point absorber wave energy converters in irregular waves. Ocean. Eng. 173, 716–731.

Boren, B.C., Lomonaco, P., Batten, B.A., Paasch, R.K., 2016. Design, development, and testing of a scaled vertical axis pendulum wave energy converter. IEEE Trans. Sustain. Energy 8, 155–163.

Bozzi, S., Miquel, A.M., Antonini, A., Passoni, G., Archetti, R., 2013. Modeling of a point absorber for energy conversion in Italian seas. Energies 6, 3033–3051.

Chakrabarti, S.K., 1999. Modeling Laws in Ocean Engineering. Developments in Offshore Engineering. Elsevier.

Drew, B., Plummer, A.R., Sahinkaya, M.N., 2009. A review of wave energy converter technology. In: Proceedings of the Institution of Mechanical Engineers, Part A: Journal of Power and Energy, vol. 223, pp. 887–902.

Engström, J., Kurupath, V., Isberg, J., Leijon, M., 2011. A resonant two body system for a point absorbing wave energy converter with direct-driven linear generator. J. Appl. Phys. 110, 124904.

Falcão, A.F.D.O., 2010. Wave energy utilization: a review of the technologies. Renew. Sustain. Energy Rev. 14, 899–918.

Falnes, J., 1999. Wave-energy conversion through relative motion between two single-mode oscillating bodies. J. Offshore Mech. Arctic Eng. 121, 32–38.

Falnes, J., Kurniawan, A., 2020. Ocean Waves and Oscillating Systems: Linear Interactions Including Wave-Energy Extraction. Cambridge university press.

Gaspar, J.F., Calvário, M., Kamarlouei, M., Soares, C.G., 2018. Design tradeoffs of an oil-hydraulic power take-off for wave energy converters. Renew. Energy 129, 245–259.

Goggins, J., Finnegan, W., 2014. Shape optimisation of floating wave energy converters for a specified wave energy spectrum. Renew. Energy 71, 208–220.

Golbaz, D., Asadi, R., Amini, E., Mehdipour, H., Nasiri, M., Nezhad, M.M., Naeeni, S.T.O., Neshat, M., 2021. Ocean Wave Energy Converters Optimization: A Comprehensive Review on Research Directions arXiv preprint arXiv:2105.07180.

Haraguchi, R., Asai, T., 2020. Enhanced power absorption of a point absorber wave energy converter using a tuned inertial mass. Energy 202, 117740.

Hong, Y., Waters, R., Boström, C., Eriksson, M., Engström, J., Leijon, M., 2014. Review on electrical control strategies for wave energy converting systems. Renew. Sustain. Energy Rev. 31, 329–342.

Hudspeth, R.T., 2006. Waves and Wave Forces on Coastal and Ocean Structures. World scientific.

Jama, M., Wahyudie, A., Noura, H., 2018. Robust predictive control for heaving wave energy converters. Control Eng. Pract. 77, 138–149.

Jin, P., Zhou, B., Göteman, M., Chen, Z., Zhang, L., 2019. Performance optimization of a coaxial-cylinder wave energy converter. Energy 174, 450–459.

Khuri, A.I., Mukhopadhyay, S., 2010. Response Surface Methodology. Wiley Interdisciplinary Reviews: Computational Statistics, vol. 2, pp. 128–149.

Koh, H.J., Ruy, W.S., Cho, I.H., Kweon, H.M., 2015. Multi-objective optimum design of a buoy for the resonant-type wave energy converter. J. Mar. Sci. Technol. 20, 53–63.

Kurniawan, A., Moan, T., 2012. Optimal geometries for wave absorbers oscillating about a fixed axis. IEEE J. Ocean. Eng. 38, 117–130.

Li, G., Belmont, M.R., 2014. Model predictive control of sea wave energy converters–part i: a convex approach for the case of a single device. Renew. Energy 69, 453–463.

Li, X., Chen, C., Li, Q., Xu, L., Liang, C., Ngo, K., Parker, R.G., Zuo, L., 2020. A compact mechanical power take-off for wave energy converters: design, analysis, and test verification. Appl. Energy 278, 115459.

Liang, C., Zuo, L., 2017. On the dynamics and design of a two-body wave energy converter. Renew. Energy 101, 265–274.

López, M., Taveira-pinto, F., Rosa-santos, P., 2017. Influence of the power take-off characteristics on the performance of CECO wave energy converter. Energy 120, 686–697.

Massel, S.R., 2007. Ocean Waves Breaking and Marine Aerosol Fluxes. Springer Science & Business Media.

Mccabe, A., 2013. Constrained optimization of the shape of a wave energy collector by genetic algorithm. Renew. Energy 51, 274–284.

Murai, M., Sakamoto, S., 2021. The fundamental research on AI prediction and determination of control force for maximizing the power generation of PA-WEC in irregular waves. In: International Conference on Offshore Mechanics and Arctic Engineering. American Society of Mechanical Engineers, V005T05A010.

Murai, M., Funada, J., Li, Q., 2020. How the hydrodynamic response of PA-WECs' array under maximizing the power generation by its arrangement and control force change. In: International Conference on Offshore Mechanics and Arctic Engineering. American Society of Mechanical Engineers, V005T05A011.

Murai, M., Li, Q., Funada, J., 2021. Study on power generation of single Point Absorber Wave Energy Converters (PA-WECs) and arrays of PA-WECs. Renew. Energy 164, 1121–1132.

Neter, J., Kutner, M.H., Nachtsheim, C.J., Wasserman, W., 1996. Applied Linear Statistical Models.

Ocean Power Technologies, 2021. https://oceanpowertechnologies.com/.

Park, J.S., Gu, B.G., Kim, J.R., Cho, I.H., Jeong, I., Lee, J., 2016. Active phase control for maximum power point tracking of a linear wave generator. IEEE Trans. Power Electron. 32, 7651–7662.

Pastor, J., Liu, Y., 2014. Frequency and time domain modeling and power output for a heaving point absorber wave energy converter. Int. J. Energy Environ. Eng. 5, 1–13.

Payne, G.S., Taylor, J.R., Ingram, D., 2009. Best practice guidelines for tank testing of wave energy converters. J. Ocean Technol. 4, 38–70.

Ryan, B.F., Joiner, B.L., Cryer, J.D., 2012. MINITAB Handbook: Update for Release. Cengage Learning.

Shadman, M., Estefen, S.F., Rodriguez, C.A., Nogueira, I.C., 2018. A geometrical optimization method applied to a heaving point absorber wave energy converter. Renew. Energy 115, 533–546.

Sharp, C., Dupont, B., 2018. Wave energy converter array optimization: a genetic algorithm approach and minimum separation distance study. Ocean. Eng. 163, 148–156.

Sheng, W., Alcorn, R., Lewis, T., 2014. Physical modelling of wave energy converters. Ocean. Eng. 84, 29–36.

Son, D., Yeung, R.W., 2017. Optimizing ocean-wave energy extraction of a dual coaxial-cylinder WEC using nonlinear model predictive control. Appl. Energy 187, 746–757.

St, L., Wold, S., 1989. Analysis of variance (ANOVA). Chemometr. Intell. Lab. Syst. 6, 259–272.

Stoker, J.J., 2011. Water Waves: the Mathematical Theory with Applications. John Wiley & Sons.

Weber, J., Mouwen, F., Parish, A., Robertson, D., 2009. Wavebob—research & development network and tools in the context of systems engineering. In: Proc.

Eighth European Wave and Tidal Energy Conference, Uppsala, Sweden, pp. 416–420.
Wen, Y., Wang, W., Liu, H., Mao, L., Mi, H., Wang, W., Zhang, G., 2018. A shape optimization method of a specified point absorber wave energy converter for the south China sea. Energies 11, 2645.
Wilkinson, L., 2006. Revising the Pareto chart. Am. Statistician 60, 332–334.
Wu, J., Yao, Y., Zhou, L., Göteman, M., 2018. Real-time latching control strategies for the solo Duck wave energy converter in irregular waves. Appl. Energy 222, 717–728.
Yang, S., Chen, H., Ji, Z., Li, H., Xiang, X., 2021. Modelling and Analysis of Inertia Self-tuning Phase Control Strategy for a Floating Multi-body Wave Energy Converter. IET Renewable Power Generation.
Zhang, X.-T., Yang, J.-M., Xiao, L.-F., 2014. Declutching control of a point absorber with direct linear electric PTO systems. Ocean Systems Eng. 4, 63–82.
Zou, S., Abdelkhalik, O., 2020. Modeling of a variable-geometry wave energy converter. IEEE J. Ocean. Eng. 46, 879–890.